Computer Assisted Mechanics and Engineering Sciences, **15**: 289–303, 2008.

Hybrid-Trefftz stress and displacement elements for dynamic analysis of bounded and unbounded saturated porous media

Ionuţ D. Moldovan
Universidade Católica Portuguesa, Department of Engineering
Estrada Octávio Pato, 2635-631, Rio de Mouro, Portugal

João A. Teixeira de Freitas
Instituto Superior Técnico, Department of Civil Engineering and Architecture
Avenida Rovisco Pais, 1049-001, Lisboa, Portugal

(Received in the final form November 18, 2008)

The displacement and stress models of the hybrid-Trefftz finite element formulation are applied to the dynamic analysis of two-dimensional bounded and unbounded saturated porous media problems. The formulation develops from the classical separation of variables in time and space. A finite element approach is used for the discretization in time of the governing differential equations. It leads to a series of uncoupled problems in the space dimension, each of which is subsequently discretized using either the displacement or the stress model of the hybrid-Trefftz finite element formulation. As typical of the Trefftz methods, the domain approximation bases are constrained to satisfy locally all domain equations. An absorbing boundary element is adopted in the extension to the analysis of unbounded media. The paper closes with the illustration of the application of the alternative hybrid-Trefftz stress and displacement elements to the solution of bounded and unbounded consolidation problems.

1. Introduction

In 1926, E. Trefftz [33] suggested using trial functions satisfying *a priori* the governing differential equations, as an alternative to the well-known Rayleigh-Ritz method. While the earliest applications involving Trefftz-type elements date from 1973 [30, 31], their use was confined to particular parts of the domain, the rest being analyzed via conventional finite elements. The first general purpose, domain-independent, Trefftz elements emerged in 1978 [19], when J. Jirousek presented four hybrid-Trefftz formulations, differing essentially in terms of the fields independently approximated on the boundaries and in the way the inter-element continuity was enforced. The early applications of these elements dealt with general plane elasticity problems [22] and Kirchhoff plates [21, 22]. The formulation was then further extended to the analysis of thin shells [20, 34], of Reissner–Mindlin plates [21, 25] and of thick plates [24, 25]. In 1980, I. Herrera published the first [14] out of a series of articles (e.g. [13, 15]) providing the mathematical fundamentals needed for building complete Trefftz bases and for using them reliably. Later, also integrated in a monograph [16], the theory developed by I. Herrera pivots on a completeness criterion, and also includes, among other concepts, convergence conditions and variational principles. Subsequently, the same approach applied to problems involving non-symmetric differential operators has led to the formulation of the Localized Adjoint Method [17], thus supporting the use of discontinuous Trefftz functions. Apart from the original hybrid-Trefftz formulations contributed by J. Jirousek, independent lines in terms of development and implementation have been proposed. The method suggested by Cheung [4], known as the direct Trefftz formulation, as opposed to the indirect one originally contributed by J. Jirousek, derives

a boundary integral expression by enforcing in a weak form the governing differential equation using the TH-complete basis for weighting. The boundary integral equation is then discretized and solved using the classical boundary element method strategy [5, 18]. This approach casts insight into the intimate relations between the Trefftz formulations and the boundary element method, allowing one to apprehend the first as a subclass of the latter. On the contrary, the hybrid-Trefftz finite elements reported in [6, 9–12, 28] are built upon their understanding as a variant of the hybrid finite elements [7] with the essential characteristic that the domain approximation basis is being built on a function space taken from the solution set of the governing differential equation. The latter concept is used throughout the work reported here. Reviews on the hybrid-Trefftz element formulations and their application can be found, for instance, in [23, 26, 29].

This paper reports on the formulation of hybrid-Trefftz displacement and stress elements for non-periodic and transient saturated porous media problems. The model assumes an elastic solid phase fully permeated by a compressible liquid phase obeying Darcy's law. The Biot's theory of porous media [2] is used to express the differential equations governing the problem. Their integration involves the uncoupling of the temporal and spatial components of the unknown fields, followed by a time domain semi-discretization process [8] to yield a series of elliptic differential equations in spatial variables only. Each of the resulting problems in space is subsequently discretized using either the displacement or the stress model of the hybrid-Trefftz formulation. The hybrid-Trefftz displacement (stress) element is naturally derived from its purely hybrid correspondent by enforcing the Trefftz constraint, requiring that the approximation functions selected for the domain displacement (stress) field satisfy the Navier (Beltrami) differential equation, into the domain equilibrium and elasticity (compatibility and elasticity) equations. A Robin-type boundary condition, relating the far-field asymptotic expressions of the displacement and traction fields [28], is enforced at close-range to yield a local absorbing boundary condition. An analysis of its effectiveness in damping incident waves of various types can be found in [27]. To illustrate the performance of the presented hybrid-Trefftz models, they are applied to plane Molsand soil consolidation problems, defined on both bounded and unbounded domains. The predicted behavior is assessed from the perspective of the consolidation theory and is compared with the results obtained with $ABAQUS^{TM}$.

2. Problem description

Let V represent a saturated porous medium and let Γ be its surface (Fig. 1), combining the complementary Neumann Γ_σ and Dirichlet Γ_u boundaries, whereon the components of the traction $\boldsymbol{t}_\Gamma$ or displacement $\boldsymbol{u}_\Gamma$ vectors are prescribed, respectively,

$$\Gamma = \Gamma_\sigma \cup \Gamma_u\,,$$
$$\phi = \Gamma_\sigma \cap \Gamma_u\,.$$

No particular constraints are enforced on the geometry of the domain, which may not be convex, simply connected or bounded. Problems defined on unbounded domains can be dealt with by artificially splitting the domain V into a bounded part, enclosing all geometric irregularities, all sources of perturbation and the whole domain of practical interest, denominated herein *interior domain*, V_{int} and an infinite sector, called *exterior domain*, V_{ext}, which is generally not included in the calculation. The delimitation is done through an imaginary boundary Γ_a, named *absorbing boundary*.

Let the independent components of the stress and strain tensors in the solid phase and the pore fluid pressure (π) and fluid content (ζ) be organized in vectors $\boldsymbol{\sigma}(x,y,t) = \{\,\sigma_{xx}\ \sigma_{yy}\ \sigma_{xy}\ \pi\,\}^T$ and $\boldsymbol{\varepsilon} = \{\,\varepsilon_{xx}\ \varepsilon_{yy}\ 2\varepsilon_{xy}\ \zeta\,\}^T$, respectively, and let the solid skeleton displacement and fluid seepage components be collected in the displacement vector $\boldsymbol{u}(x,y,t) = \{\,u_x\ u_y\ w_x\ w_y\,\}^T$. The total components of the body forces are listed in the body force vector $\boldsymbol{b}(x,y,t) = \{\,\rho b_x\ \rho b_y\ \rho_w b_x\ \rho_w b_y\,\}^T$, where ρ and ρ_w represent the mass density of the mixture and of the liquid phase, respectively, while b_x and b_y are the components of the body force.

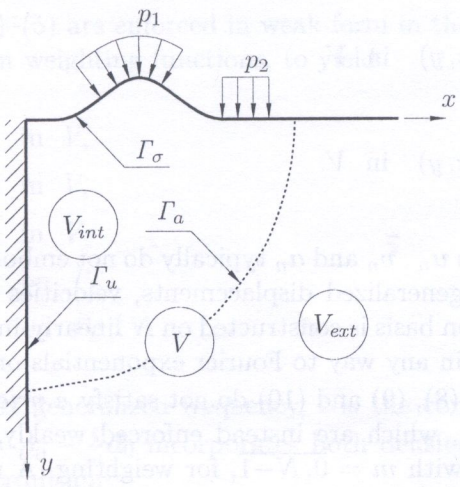

Fig. 1. Interior and exterior domains, Neumann, Dirichlet and Sommerfeld boundaries

The linear elastodynamic response of the body is governed by the following differential equations, written in the matrix form

$$\mathcal{D}\boldsymbol{\sigma} + \boldsymbol{b} = \boldsymbol{d}_0\dot{\boldsymbol{u}} + \boldsymbol{\rho}_0\ddot{\boldsymbol{u}} \quad \text{in } V, \tag{1}$$

$$\boldsymbol{\varepsilon} = \mathcal{D}^*\boldsymbol{u} \quad \text{in } V, \tag{2}$$

$$\boldsymbol{\sigma} = \boldsymbol{k}\boldsymbol{\varepsilon} \quad \text{in } V, \tag{3}$$

$$\boldsymbol{N}\boldsymbol{\sigma} = \boldsymbol{t}_\Gamma \quad \text{on } \Gamma_\sigma, \tag{4}$$

$$\boldsymbol{u} = \boldsymbol{u}_\Gamma \quad \text{on } \Gamma_u. \tag{5}$$

In the equilibrium (1), compatibility (2) and elasticity (3) equations, the dynamic properties of the body are collected in the (local, symmetric) density $\boldsymbol{\rho}_0(x,y)$ and structural damping $\boldsymbol{d}_0(x,y)$ matrices, while the (local, symmetric) matrix $\boldsymbol{k}(x,y)$ defines its elastic properties. Matrices $\mathcal{D}$ and $\mathcal{D}^*$ are the differential equilibrium and compatibility operators, respectively. The explicit expressions of these matrices for saturated porous media can be found in [27].

Vectors $\boldsymbol{t}_\Gamma(x,y,t) = \left\{ t_{\Gamma_x}\ t_{\Gamma_y}\ \pi_\Gamma \right\}^T$ and $\boldsymbol{u}_\Gamma(x,y,t) = \left\{ u_{\Gamma_x}\ u_{\Gamma_y}\ w_{\Gamma_n} \right\}^T$, present in boundary equilibrium (4) and compatibility (5) equations, collect the components of the applied tractions (applied pore pressure, for the fluid phase) and of the imposed displacements (imposed normal seepage), respectively. The components of the outward normal to the medium boundary are organized in matrix $\boldsymbol{N}$.

The initial displacements and velocities of the dynamic system are known *a priori* and their components collected in vectors $\boldsymbol{u}^0(x,y)$ and $\boldsymbol{v}^0(x,y)$, respectively:

$$\boldsymbol{u} = \boldsymbol{u}^0 \quad \text{at } t = 0, \tag{6}$$

$$\dot{\boldsymbol{u}} = \boldsymbol{v}^0 \quad \text{at } t = 0. \tag{7}$$

3. Time discretization

The discretization in time of the governing equations is constructed using the finite element procedure reported in [8]. Let the analysis duration be split into a certain number of time steps. Direct approximations are assumed in the current time step ($0 \le t \le \Delta t$) for the unknown displacement, velocity and acceleration fields,

$$\boldsymbol{u}(x,y,t) = \sum_{n=0}^{N-1} W_n(t)\,\boldsymbol{u}_n(x,y) \quad \text{in } V, \tag{8}$$

$$\boldsymbol{v}(x,y,t) = \sum_{n=0}^{N-1} W_n(t)\,\boldsymbol{v}_n(x,y) \quad \text{in } V, \tag{9}$$

$$\boldsymbol{a}(x,y,t) = \sum_{n=0}^{N-1} W_n(t)\,\boldsymbol{a}_n(x,y) \quad \text{in } V. \tag{10}$$

In the above equations, weights $\boldsymbol{u}_n$, $\boldsymbol{v}_n$ and $\boldsymbol{a}_n$ typically do not embody field values at given moments in time, representing instead generalized displacements, velocities and accelerations, respectively. The time domain approximation basis is constructed on N linearly-independent scalar functions W_n, whose choice is not restricted in any way to Fourier exponentials or any other function space.

In general, approximations (8), (9) and (10) do not satisfy *a priori* the velocity and acceleration definitions $\dot{\boldsymbol{u}} = \boldsymbol{v}$ and $\dot{\boldsymbol{v}} = \boldsymbol{a}$, which are instead enforced weakly, using the (complex conjugate of the) scalar functions W_m, with $m = \overline{0, N-1}$, for weighting. A number of N uncoupled sets of equations of type (11) and (12) are obtained,

$$\int_0^{\Delta t} \widehat{W_m}(\boldsymbol{v} - \dot{\boldsymbol{u}})\,\mathrm{d}t = \boldsymbol{0}, \tag{11}$$

$$\int_0^{\Delta t} \widehat{W_m}(\boldsymbol{a} - \dot{\boldsymbol{v}})\,\mathrm{d}t = \boldsymbol{0}. \tag{12}$$

Applying the procedure presented in [8], the following velocity and acceleration estimates are obtained,

$$\Delta t\,\boldsymbol{v}(t) = \sum_{n=0}^{N-1} W_n(t)\;\Psi_n \boldsymbol{u}_n - \theta_0(t)\boldsymbol{u}^0, \tag{13}$$

$$\Delta t^2 \boldsymbol{a}(t) = \sum_{n=0}^{N-1} W_n(t)\;\Psi_n^2 \boldsymbol{u}_n - \theta_1(t)\,\boldsymbol{u}^0 - \theta_0(t)\Delta t\,\boldsymbol{v}^0, \tag{14}$$

where

$$\theta_k(t) = \sum_{n=0}^{N-1} W_n(t)\;\Psi_n^k \psi_n,$$

$$\psi_n = \sum_{m=0}^{N-1} \overline{H_{nm}}\,\widehat{W_m}(0),$$

and Ψ_n, ψ_n and $\overline{H_{nm}}$ are constants depending on the approximation basis.

Besides the displacement field (8), the time variation functions of the unknown strain and stress fields are directly approximated in the current time step ($0 \le t \le \Delta t$) using the same arbitrary time basis $W_n(t)$,

$$\boldsymbol{\varepsilon}(x,y,t) = \sum_{n=0}^{N-1} W_n(t)\,\boldsymbol{\varepsilon}_n(x,y) \quad \text{in } V \tag{15}$$

$$\boldsymbol{\sigma}(x,y,t) = \sum_{n=0}^{N-1} W_n(t)\,\boldsymbol{\sigma}_n(x,y) \quad \text{in } V \tag{16}$$

and the governing equations (1)–(5) are enforced in weak form in the same time interval, using the scalar functions W_m as Galerkin weighting functions, to yield

$$\boldsymbol{\mathcal{D}}\boldsymbol{\sigma}_n + \boldsymbol{b}_n + \omega_n^2 \boldsymbol{\rho}\boldsymbol{u}_n = \boldsymbol{F}_n^0 \quad \text{in } V, \tag{17}$$

$$\boldsymbol{\varepsilon}_n = \boldsymbol{\mathcal{D}}^* \boldsymbol{u}_n \quad \text{in } V, \tag{18}$$

$$\boldsymbol{\sigma}_n = \boldsymbol{k}\boldsymbol{\varepsilon}_n \quad \text{in } V, \tag{19}$$

$$\boldsymbol{N}\boldsymbol{\sigma}_n - \boldsymbol{t}_{\Gamma_n} = \boldsymbol{0} \quad \text{on } \Gamma_\sigma, \tag{20}$$

$$\boldsymbol{u}_n = \boldsymbol{u}_{\Gamma_n} \quad \text{on } \Gamma_u, \tag{21}$$

where $\omega_n = -\hat{\imath}\frac{\Psi_n}{\Delta t}$ is a complex generalized frequency, $\hat{\imath}$ is the complex imaginary unit, and the generalized density matrix $\boldsymbol{\rho} = \boldsymbol{\rho}_0 - \frac{\hat{\imath}}{\omega}\boldsymbol{d}_0$ incorporates both density ($\boldsymbol{\rho}_0$) and structural damping ($\boldsymbol{d}_0$) effects and is no longer Hermitian.

The generalized forces associated with the initial conditions (6) and (7), the generalized body forces and the contributions of the prescribed forces and displacements are defined as follows,

$$\boldsymbol{F}_n^0 = -\frac{\psi_n}{\Delta t}\left(\hat{\imath}\omega_n \boldsymbol{\rho}\boldsymbol{u}^0 + \boldsymbol{\rho}_0 \boldsymbol{v}^0\right), \tag{22}$$

$$\boldsymbol{b}_n = \frac{1}{\Delta t}\sum_{m=0}^{N-1} \overline{H_{nm}} \int_0^{\Delta t} \widehat{W_m}\boldsymbol{b}\,\mathrm{d}t, \tag{23}$$

$$\boldsymbol{t}_{\Gamma_n} = \frac{1}{\Delta t}\sum_{m=0}^{N-1} \overline{H_{nm}} \int_0^{\Delta t} \widehat{W_m}\boldsymbol{t}_\Gamma\,\mathrm{d}t, \tag{24}$$

$$\boldsymbol{u}_{\Gamma_n} = \frac{1}{\Delta t}\sum_{m=0}^{N-1} \overline{H_{nm}} \int_0^{\Delta t} \widehat{W_m}\boldsymbol{u}_\Gamma\,\mathrm{d}t. \tag{25}$$

Substituting the compatible strain field given by Eq. (18) in the elasticity equation (19) and the resulting stress field in the equilibrium condition (17), the Navier equation results in the form

$$\boldsymbol{\mathcal{D}}\boldsymbol{k}\boldsymbol{\mathcal{D}}^*\boldsymbol{u}_n + \boldsymbol{b}_n + \omega_n^2\boldsymbol{\rho}\boldsymbol{u}_n = \boldsymbol{F}_n^0 \quad \text{in } V. \tag{26}$$

Though no provisions were postulated for the analyzed problem, which may be discontinuous and of non-repetitive nature, nor were any restraining conditions placed on the selection of the time basis W_n, which may be defined on any complete function basis, the semi-discretized domain (17), (18), (19) and boundary (20) and (21) equations are rather similar (except for the initial field vector $\boldsymbol{F}_n^0$) to their spectral forms, obtained for periodic problems via discrete Fourier transform and reported in [28]. This observation opens the possibility of analyzing any kind of phenomenon, regardless of its steadiness, using the same, spectral-like resolution algorithm.

4. Space discretization

The hybrid-Trefftz displacement and stress elements for the space discretization of the "spectral" problems defined by Eqs. (17)–(21) are obtained from the correspondent hybrid formulations requiring that the approximation functions in space satisfy the homogeneous form of the domain differential equations [7, 27]. In the following derivations, the subscript n associated with the current "spectral" problem is dropped for notation convenience.

4.1. Trefftz compliant approximation bases

Let the displacement field in the domain of a displacement element be approximated as

$$\boldsymbol{u} = \boldsymbol{U}\boldsymbol{X} + \boldsymbol{u}_0 \quad \text{in } V. \tag{27}$$

In Eq. (27), vector $\boldsymbol{X}$ collects the generalized displacements associated with the functions listed in the matrix $\boldsymbol{U}$, while vector $\boldsymbol{u}_0$ collects particular solutions usually associated with the body forces and with the initial condition vector.

What typifies the Trefftz formulation is the requirement that the functions collected in the basis $\boldsymbol{U}$ satisfy locally the homogeneous form of the domain equations. This condition is secured by solving the homogeneous form of the Navier equation (26) and using its complete set of solutions as approximation functions. Consequently, the following expression holds,

$$\left(\mathcal{D}\boldsymbol{k}\mathcal{D}^* + \omega^2\boldsymbol{\rho}\right)\boldsymbol{U} = \boldsymbol{0}. \tag{28}$$

Dependent bases can be formulated for the approximation of the domain strain and stress fields

$$\boldsymbol{\varepsilon} = \boldsymbol{E}\boldsymbol{X} + \boldsymbol{\varepsilon}_0 \quad \text{in } V, \tag{29}$$

$$\boldsymbol{\sigma} = \boldsymbol{S}\boldsymbol{X} + \boldsymbol{\sigma}_0 \quad \text{in } V, \tag{30}$$

where the approximation bases $\boldsymbol{E}$ and $\boldsymbol{S}$ are derived from the displacement basis $\boldsymbol{U}$ such to satisfy locally the compatibility (18) and equilibrium (17) equations, respectively. It follows that the elasticity equation (19) must be also locally observed, and thus the following properties of the resulting Trefftz basis can be stated,

$$\boldsymbol{E} = \mathcal{D}^*\boldsymbol{U}, \tag{31}$$

$$\boldsymbol{S} = \boldsymbol{k}\boldsymbol{E}, \tag{32}$$

$$\mathcal{D}\boldsymbol{S} + \omega^2\boldsymbol{\rho}\boldsymbol{U} = \boldsymbol{0}. \tag{33}$$

The particular solution vectors $\boldsymbol{u}_0$, $\boldsymbol{\varepsilon}_0$ and $\boldsymbol{\sigma}_0$ present in definitions (27), (29) and (30), respectively, may, but do not necessarily do satisfy the non-homogeneous form of the Navier equation (26). Nevertheless, they are subjected to the traditional constraint of (pure-)hybrid formulations which requires that for a displacement (stress) model the domain strain (stress) field locally satisfies the domain compatibility (equilibrium) condition

$$\boldsymbol{\varepsilon}_0 = \mathcal{D}^*\boldsymbol{u}_0 \qquad \text{for the displacement model,} \tag{34}$$

$$\mathcal{D}\boldsymbol{\sigma}_0 + \omega^2\boldsymbol{\rho}\boldsymbol{u}_0 = \boldsymbol{F}^0 - \boldsymbol{b} \qquad \text{for the stress model.} \tag{35}$$

Bounded to satisfy locally the all domain equations, the relation between the domain displacement (27) and stress (30) fields is unique. Thus, the distinction between the definitions of the displacement and stress approximation bases, $\boldsymbol{U}$ and $\boldsymbol{S}$, used as primary bases for the displacement and for the stress models, respectively, can only be formal, in the sense that for the displacement model the displacement approximation is direct and the stress basis is derived such to satisfy locally the equilibrium equation, while the opposite is true for the stress model. For saturated porous media, the derivation of the approximation bases is given in [27].

4.2. Displacement element

Apart from the domain displacement field approximation (27), the traction field is independently approximated on the Dirichlet boundary Γ_u, as

$$\boldsymbol{t} = \boldsymbol{Z}\boldsymbol{p} \quad \text{on } \Gamma_u. \tag{36}$$

The functions used to define the (strictly hierarchical) boundary traction basis Z only bear the restrictions of completeness and linear independence.

The finite element equilibrium equation

$$\boldsymbol{D}\boldsymbol{X} - \boldsymbol{B}\boldsymbol{p} = \overline{\boldsymbol{t}_{\Gamma}^{u}} - \overline{\boldsymbol{t}_{\Gamma_0}^{u}} + \overline{\boldsymbol{F}_0}\,, \tag{37}$$

where

$$\boldsymbol{D} = \int \widehat{\boldsymbol{U}}^T \boldsymbol{N}\boldsymbol{S}\,\mathrm{d}\Gamma\,, \tag{38}$$

$$\boldsymbol{B} = \int \widehat{\boldsymbol{U}}^T \boldsymbol{Z}\,\mathrm{d}\Gamma_u\,, \tag{39}$$

$$\overline{\boldsymbol{t}_{\Gamma}^{u}} = \int \widehat{\boldsymbol{U}}^T \boldsymbol{t}_{\Gamma}\,\mathrm{d}\Gamma_\sigma\,, \tag{40}$$

$$\overline{\boldsymbol{t}_{\Gamma_0}^{u}} = \int \widehat{\boldsymbol{U}}^T \boldsymbol{N}\boldsymbol{\sigma}_0\,\mathrm{d}\Gamma, \tag{41}$$

$$\overline{\boldsymbol{F}_0} = \int \widehat{\boldsymbol{U}}^T \left(\mathcal{D}\boldsymbol{\sigma}_0 + \boldsymbol{b} + \omega^2\rho\boldsymbol{u}_0 - \boldsymbol{F}^0\right)\mathrm{d}V, \tag{42}$$

is derived by imposing on average the equilibrium condition (17),

$$\int \widehat{\boldsymbol{U}}^T \left(\mathcal{D}\boldsymbol{\sigma} + \boldsymbol{b} + \omega^2\rho\boldsymbol{u}\right)\mathrm{d}V = \int \widehat{\boldsymbol{U}}^T \boldsymbol{F}^0\,\mathrm{d}V, \tag{43}$$

integrating by parts the above equation, substituting the field approximations (27) and (30), and explicitly enforcing condition (20) on the Neumann boundary and approximation (36) on the Dirichlet boundary.

The finite element displacement compatibility equation is derived by enforcing on average the Dirichlet boundary condition (21) using the traction approximation functions defined in Eq. (36) as weighting functions

$$\int \widehat{\boldsymbol{Z}}^T (\boldsymbol{u} - \boldsymbol{u}_\Gamma)\,\mathrm{d}\Gamma_u = \boldsymbol{0}. \tag{44}$$

Substituting the displacement approximation (27), one gets

$$\widehat{\boldsymbol{B}}^T \boldsymbol{X} = \overline{\boldsymbol{u}_{\Gamma}^{u}} - \overline{\boldsymbol{u}_{\Gamma_0}^{u}}\,, \tag{45}$$

where

$$\overline{\boldsymbol{u}_{\Gamma}^{u}} = \int \widehat{\boldsymbol{Z}}^T \boldsymbol{u}_\Gamma\,\mathrm{d}\Gamma_u\,, \tag{46}$$

$$\overline{\boldsymbol{u}_{\Gamma_0}^{u}} = \int \widehat{\boldsymbol{Z}}^T \boldsymbol{u}_0\,\mathrm{d}\Gamma_u\,. \tag{47}$$

Equations (37) and (45) are used to construct the finite element governing system as

$$\begin{bmatrix} \boldsymbol{D} & -\boldsymbol{B} \\ -\widehat{\boldsymbol{B}}^T & \boldsymbol{0} \end{bmatrix} \begin{bmatrix} \boldsymbol{X} \\ \boldsymbol{p} \end{bmatrix} = \begin{bmatrix} \overline{\boldsymbol{t}_{\Gamma}^{u}} - \overline{\boldsymbol{t}_{\Gamma_0}^{u}} + \overline{\boldsymbol{F}_0} \\ \overline{\boldsymbol{u}_{\Gamma_0}^{u}} - \overline{\boldsymbol{u}_{\Gamma}^{u}} \end{bmatrix}. \tag{48}$$

4.3. Stress element

Apart from the domain stress field approximation (30), the displacement field is independently approximated on the Neumann boundary Γ_σ, as

$$\boldsymbol{u} = \boldsymbol{Z}\boldsymbol{q} \quad \text{on } \Gamma_\sigma\,. \tag{49}$$

The functions used to define the (strictly hierarchical) boundary displacement basis $\boldsymbol{Z}$ only bear the restrictions of completeness and linear independence.

The finite element compatibility equation is derived by imposing on average the compatibility condition (18),

$$\int \widehat{\boldsymbol{S}}^T (\boldsymbol{\varepsilon} - \boldsymbol{\mathcal{D}}^* \boldsymbol{u}) \, \mathrm{d}V = \boldsymbol{0}. \tag{50}$$

Integrating by parts the above equation, substituting the field approximations (29) and (30), and explicitly enforcing condition (21) on the Dirichlet boundary term and approximation (49) on the Neumann boundary, the following expression is obtained,

$$\widehat{\boldsymbol{D}}^T \boldsymbol{X} - \boldsymbol{A}\boldsymbol{q} = \overline{\boldsymbol{u}_{\Gamma}^{\sigma}} - \overline{\boldsymbol{u}_{\Gamma_0}^{\sigma}} + \overline{\boldsymbol{U}_0}, \tag{51}$$

$$\boldsymbol{A} = \int (\boldsymbol{N}\widehat{\boldsymbol{S}})^T \boldsymbol{Z} \, \mathrm{d}\Gamma_{\sigma}, \tag{52}$$

$$\overline{\boldsymbol{u}_{\Gamma}^{\sigma}} = \int (\boldsymbol{N}\widehat{\boldsymbol{S}})^T \boldsymbol{u}_{\Gamma} \, \mathrm{d}\Gamma_{u}, \tag{53}$$

$$\overline{\boldsymbol{u}_{\Gamma_0}^{\sigma}} = \int (\boldsymbol{N}\widehat{\boldsymbol{S}})^T \boldsymbol{u}_0 \, \mathrm{d}\Gamma, \tag{54}$$

$$\overline{\boldsymbol{U}_0} = \int \widehat{\boldsymbol{S}}^T (\boldsymbol{\mathcal{D}}^* \boldsymbol{u}_0 - \boldsymbol{\varepsilon}_0) \, \mathrm{d}V. \tag{55}$$

The finite element boundary equilibrium equation is derived by enforcing on average the Neumann boundary condition (20) using the traction approximation functions defined in Eq. (49) as weighting functions,

$$\int \widehat{\boldsymbol{Z}}^T (\boldsymbol{N}\boldsymbol{\sigma} - \boldsymbol{t}_{\Gamma}) \, \mathrm{d}\Gamma_{\sigma} = \boldsymbol{0}. \tag{56}$$

Substituting the stress approximation (30), one gets

$$\widehat{\boldsymbol{A}}^T \boldsymbol{X} = \overline{\boldsymbol{t}_{\Gamma}^{\sigma}} - \overline{\boldsymbol{t}_{\Gamma_0}^{\sigma}}, \tag{57}$$

where

$$\overline{\boldsymbol{t}_{\Gamma}^{\sigma}} = \int \widehat{\boldsymbol{Z}}^T \boldsymbol{t}_{\Gamma} \, \mathrm{d}\Gamma_{\sigma}, \tag{58}$$

$$\overline{\boldsymbol{t}_{\Gamma_0}^{\sigma}} = \int \widehat{\boldsymbol{Z}}^T \boldsymbol{N}\boldsymbol{\sigma}_0 \, \mathrm{d}\Gamma_{\sigma}. \tag{59}$$

Equations (51) and (57) are used to construct the finite element governing system as,

$$\begin{bmatrix} \widehat{\boldsymbol{D}}^T & -\boldsymbol{A} \\ -\widehat{\boldsymbol{A}}^T & \boldsymbol{0} \end{bmatrix} \begin{bmatrix} \boldsymbol{X} \\ \boldsymbol{q} \end{bmatrix} = \begin{bmatrix} \overline{\boldsymbol{u}_{\Gamma}^{\sigma}} - \overline{\boldsymbol{u}_{\Gamma_0}^{\sigma}} + \overline{\boldsymbol{U}_0} \\ \overline{\boldsymbol{t}_{\Gamma_0}^{\sigma}} - \overline{\boldsymbol{t}_{\Gamma}^{\sigma}} \end{bmatrix}. \tag{60}$$

For either model, the governing system results highly sparse and strongly localized, as vectors $\boldsymbol{X}$ list the degrees of freedom associated with each structural element, thus being strictly element dependent, while vectors $\boldsymbol{p}$ and $\boldsymbol{q}$, present in Eqs. (48) and (60), respectively, are shared by at most two neighboring elements.

4.4. Absorbing boundary elements

Half-space problems are treated by artificially splitting the domain V into a bounded part, V_{int}, enclosing the region of practical interest, and an infinite sector, V_{ext}, which is not included in the

calculation. The delimitation is done by means of an imaginary boundary Γ_a (absorbing boundary), which must be designed such to prevent the spurious reflection of the incident waves back into the interior domain. To secure this, the far-field asymptotic expressions of the functions collected in the domain displacement and stress approximation bases can be used to formulate the following Robin-type relation,

$$\boldsymbol{t} = \boldsymbol{C}\boldsymbol{u} \quad \text{at far-field.} \tag{61}$$

In the above equation, $\boldsymbol{C}$ is a matrix of constants, depending on the specific characteristics of the analyzed elastic medium. Its expression for saturated porous media can be found in [27].

Condition (61) is strictly true if only the absorbing boundary Γ_a is placed infinitely far from the source of perturbation. On the other hand, placing the absorbing boundary at close-range generally renders Eq. (61) inexact, that is, its enforcement generally does not guarantee the absence of spurious reflected waves. However, as shown in [27], its damping capacity, depending on the kind and frequency of the incident wave, is sufficiently good for practical situations.

4.4.1. Displacement element with absorbing boundary

The displacement element absorbing boundary equation is derived by directly approximating the traction field (62) on Γ_a and by subsequently enforcing on average condition (61) using the (hierarchical) basis $\boldsymbol{Z}_a$ for weighting,

$$\boldsymbol{t} = \boldsymbol{Z}_a \boldsymbol{p}_a \qquad \text{on } \Gamma_a\,, \tag{62}$$

$$\int \widehat{\boldsymbol{Z}}_a^T (\boldsymbol{u} - \boldsymbol{C}^{-1}\boldsymbol{t})\,\mathrm{d}\Gamma_a^e = \boldsymbol{0} \qquad \text{on } \Gamma_a\,. \tag{63}$$

Inserting definitions (27) and (62) into Eq. (63), one gets

$$-\widehat{\boldsymbol{B}}_a^T \boldsymbol{X} + \boldsymbol{D}_a^u \boldsymbol{p}_a = \overline{\boldsymbol{u}_{a0}}\,, \tag{64}$$

where

$$\boldsymbol{B}_a = \int \widehat{\boldsymbol{U}}^T \boldsymbol{Z}_a\,\mathrm{d}\Gamma_a\,, \tag{65}$$

$$\boldsymbol{D}_a^u = \int \widehat{\boldsymbol{Z}}_a^T \boldsymbol{C}^{-1} \boldsymbol{Z}_a\,\mathrm{d}\Gamma_a\,, \tag{66}$$

$$\overline{\boldsymbol{u}_{a0}} = \int \widehat{\boldsymbol{Z}}_a^T \boldsymbol{u}_0\,\mathrm{d}\Gamma_a\,. \tag{67}$$

Equation (64) can be included into expression (48) to obtain the following form for the governing system,

$$\begin{bmatrix} \boldsymbol{D} & -\boldsymbol{B}_a & -\boldsymbol{B} \\ -\widehat{\boldsymbol{B}}_a^T & \boldsymbol{D}_a^u & \boldsymbol{0} \\ -\widehat{\boldsymbol{B}}^T & \boldsymbol{0} & \boldsymbol{0} \end{bmatrix} \begin{bmatrix} \boldsymbol{X} \\ \boldsymbol{p}_a \\ \boldsymbol{p} \end{bmatrix} = \begin{bmatrix} \overline{\boldsymbol{t}_\Gamma^u} - \overline{\boldsymbol{t}_{\Gamma_0}^u} + \overline{\boldsymbol{F}_0} \\ \overline{\boldsymbol{u}_{a0}} \\ \overline{\boldsymbol{u}_{\Gamma_0}^u} - \overline{\boldsymbol{u}_\Gamma^u} \end{bmatrix}. \tag{68}$$

4.4.2. Stress element with absorbing boundary

The stress element absorbing boundary equation is derived by directly approximating the displacement field (69) on Γ_a and by subsequently enforcing on average condition (61) using the (hierarchical) basis $\boldsymbol{Z}_a$ for weighting,

$$\boldsymbol{u} = \boldsymbol{Z}_a \boldsymbol{q}_a \qquad \text{on } \Gamma_a\,, \tag{69}$$

$$\int \widehat{\boldsymbol{Z}}_a^T (\boldsymbol{N}\boldsymbol{\sigma} - \boldsymbol{C}\boldsymbol{u})\,\mathrm{d}\Gamma_a^e = \boldsymbol{0} \qquad \text{on } \Gamma_a\,. \tag{70}$$

Inserting definitions (30) and (69) in Eq. (70), one obtains

$$-\widehat{\boldsymbol{A}}_a^T \boldsymbol{X} + \boldsymbol{D}_a^\sigma \boldsymbol{q}_a = \overline{\boldsymbol{t}_{a_0}}\,, \tag{71}$$

where

$$\boldsymbol{A}_a = \int (\boldsymbol{N}\widehat{\boldsymbol{S}})^T \boldsymbol{Z}_a \,\mathrm{d}\Gamma_a\,, \tag{72}$$

$$\boldsymbol{D}_a^\sigma = \int \widehat{\boldsymbol{Z}}_a^T \boldsymbol{C} \boldsymbol{Z}_a \,\mathrm{d}\Gamma_a\,, \tag{73}$$

$$\overline{\boldsymbol{t}_{a_0}} = \int \widehat{\boldsymbol{Z}}_a^T \boldsymbol{N}\boldsymbol{\sigma}_0 \,\mathrm{d}\Gamma_a\,. \tag{74}$$

Equation (71) can be included into expression (60) to obtain the following form for the governing system,

$$\begin{bmatrix} \widehat{\boldsymbol{D}}^T & -\boldsymbol{A}_a & -\boldsymbol{A} \\ -\widehat{\boldsymbol{A}}_a^T & \boldsymbol{D}_a^\sigma & \boldsymbol{0} \\ -\widehat{\boldsymbol{A}}^T & \boldsymbol{0} & \boldsymbol{0} \end{bmatrix} \begin{bmatrix} \boldsymbol{X} \\ \boldsymbol{q}_a \\ \boldsymbol{q} \end{bmatrix} = \begin{bmatrix} \overline{\boldsymbol{u}_\Gamma^\sigma} - \overline{\boldsymbol{u}_{\Gamma_0}^\sigma} + \overline{\boldsymbol{U}_0} \\ \overline{\boldsymbol{t}_{a_0}} \\ \overline{\boldsymbol{t}_{\Gamma_0}^\sigma} - \overline{\boldsymbol{t}_\Gamma^\sigma} \end{bmatrix}. \tag{75}$$

The generalized traction and displacement vectors $\boldsymbol{p}_a$ and $\boldsymbol{q}_a$ list the static and the kinematic degrees of freedom associated with the absorbing boundary and are strictly element dependent, as an absorbing boundary cannot be shared by two elements. Thus, the sparsity and localization features stated above for the finite element governing systems remain valid.

5. Two-dimensional consolidation tests

An external load suddenly applied on a body of saturated soil causes a local increase of the pore pressure, triggering the flow of the fluid. As the fluid leaks through the porous material, the solid skeleton suffers a gradual change in volume, a process called consolidation. Detailed theoretical treatment of the consolidation phenomenon was first given by K. Terzaghi [32], for the small strain problem. His theory was later extended to include finite strains by J.P. Carter [3].

5.1. Consolidation test on a bounded domain

The consolidation process is first modelled on the bounded two-dimensional saturated poroelastic medium presented in Fig. 2, which is subjected to a vertical load $f(x,t) = \overline{f} \cdot H(t)$, applied on the medium surface and acting exclusively on the solid phase, with $\overline{f}$ being a constant unit pressure and $H(t)$ the Heaviside time distribution. Free surface drainage is allowed for the fluid phase and the walls of the tank are considered rigid and frictionless. The material under consideration is a water-saturated Molsand soil, with a hydraulic conductivity of $k = 0.0001\,\mathrm{m/s}$. The porosity is assumed to be constant for the entire duration of the analysis. The total width of the loaded edge is $2L = 10.0\,\mathrm{m}$. Four finite elements are adopted for the spatial discretization, with a single time step to cover the duration of the test, $\Delta t = 10.0\,\mathrm{s}$. A hybrid-Trefftz stress model is used in the analysis, with the domain and boundary approximation bases built on Bessel functions of the first kind and on Tchebychev polynomials, respectively, resulting a total number of 228 static and 132 kinematic degrees of freedom. The time basis is constructed with fourth family Daubechies scaling/wavelet functions, with a resolution level of 5, which generates 64 problems in space.

Conversely, the parallel simulation implemented in $ABAQUS^{TM}$ involves the structure discretization in 100 finite elements. The finite-strain CPE4P element is used in the analysis. This is a 4-node bilinear displacement and pore pressure element, with 3 degrees of freedom per node

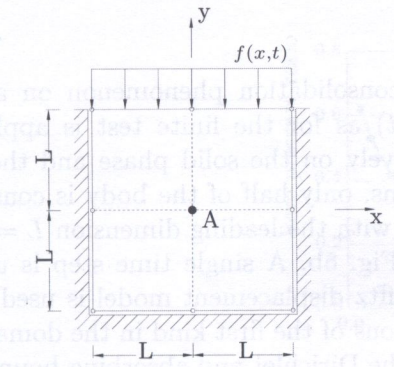

Fig. 2. Structural model for finite domain tests

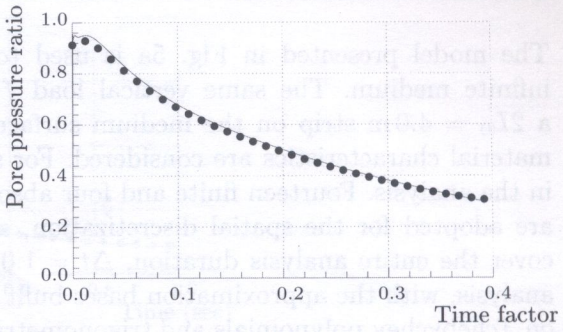

Fig. 3. Pore pressure ratio time history at point A

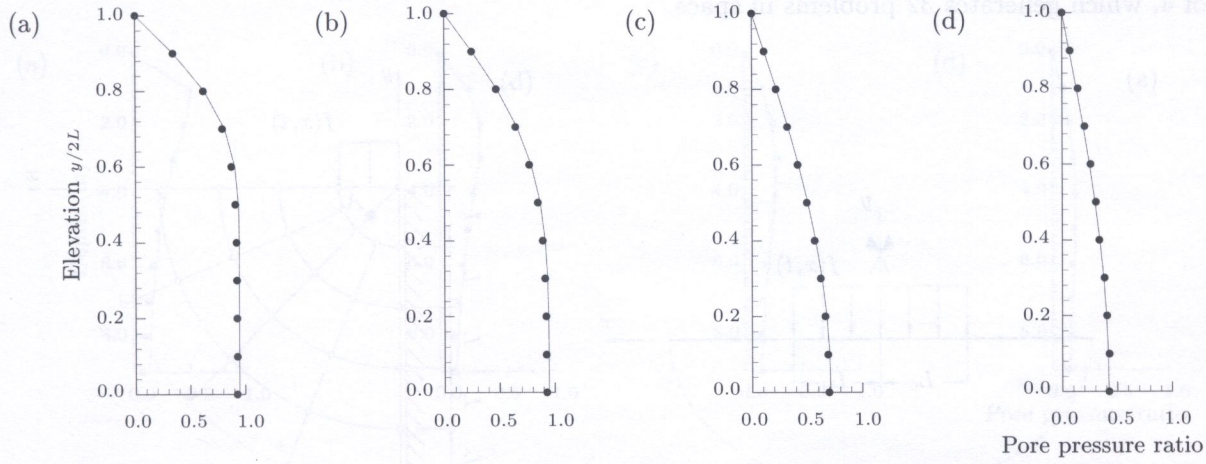

Fig. 4. Pore pressure profiles at various instants; (a) $t = 0.1\,\mathrm{s}$, (b) $t = 0.5\,\mathrm{s}$, (c) $t = 5.0\,\mathrm{s}$, (d) $t = 10.0\,\mathrm{s}$

(2 displacements and the pore pressure). Thus, the total number of structural degrees of freedom is 363. The time integration is performed applying a direct method based on the Newton's backward difference formula [1] on 250 time steps.

The time-history of the fluid pore pressure in point A is plotted in Fig. 3. For all results presented here, the hybrid-Trefftz solution is plotted with dots, while the corresponding result predicted by $ABAQUS^{TM}$ is represented by the solid line. As it is the usual practice in geomechanics [32], the pore pressure is scaled to the magnitude $\overline{f} = 1$ of the applied traction, while the non-dimensional time factor T_c is defined as $T_c = \frac{c_v t}{d^2}$, where c_v represents the consolidation coefficient and d is the length of the drainage path. Thus defined, a unit time factor roughly corresponds to the total consolidation time. It should be noted that in the initial phase of the consolidation, there exists an increase in the excess pore pressure, before it starts to dissipate. This Mandel–Cryer effect can only be captured in a two-dimensional analysis (classical one-dimensional Terzaghi consolidation test does not exhibit this trait). Its magnitude is larger when the Poisson coefficient is zero and is less important when more realistic values are adopted [32]. Subsequently, the fluid drainage predictably diminishes the excess pore pressure, first near the free surface, than gradually at greater depths in the reservoir. This process is captured by the pore pressure profiles (Fig. 4), consisting in plots of the excess pore pressures as a function of depth, at various times during the analysis. The drainage at the top surface is obvious from the initial stages of the consolidation (Fig. 4a), and a loss of pore pressure in the top region is consequently reported. The effect propagates down the reservoir until the entire medium is steadily loosing pore pressure throughout its length (Figs. 4c and 4d). The steady-state solution corresponds to zero pore pressure everywhere, with the load being entirely supported by the solid phase. In spite of the significant coarseness of the adopted temporal basis, the predicted results are clearly in good agreement with the $ABAQUS^{TM}$ solutions.

5.2. Consolidation test on a semi-infinite domain

The model presented in Fig. 5a is used to simulate the consolidation phenomenon on a semi-infinite medium. The same vertical load $f(x,t) = \overline{f} \cdot H(t)$ as for the finite test is applied on a $2L_0 = 4.0\,\mathrm{m}$ strip on the medium surface, acting exclusively on the solid phase and the same material characteristics are considered. For symmetry reasons, only half of the body is considered in the analysis. Fourteen finite and four absorbing elements, with the leading dimension $L = 2.0\,\mathrm{m}$, are adopted for the spatial discretization, as presented in Fig. 5b. A single time step is used to cover the entire analysis duration, $\Delta t = 1.0\,\mathrm{s}$. A hybrid-Trefftz displacement model is used in the analysis, with the approximation bases built on Bessel functions of the first kind in the domain and on Tchebychev polynomials and trigonometric functions on the Dirichlet and absorbing boundaries, respectively, resulting a total number of 966 kinematic and 666 static degrees of freedom. The time basis is constructed with fourth family Daubechies scaling/wavelet functions, with a resolution level of 4, which generates 32 problems in space.

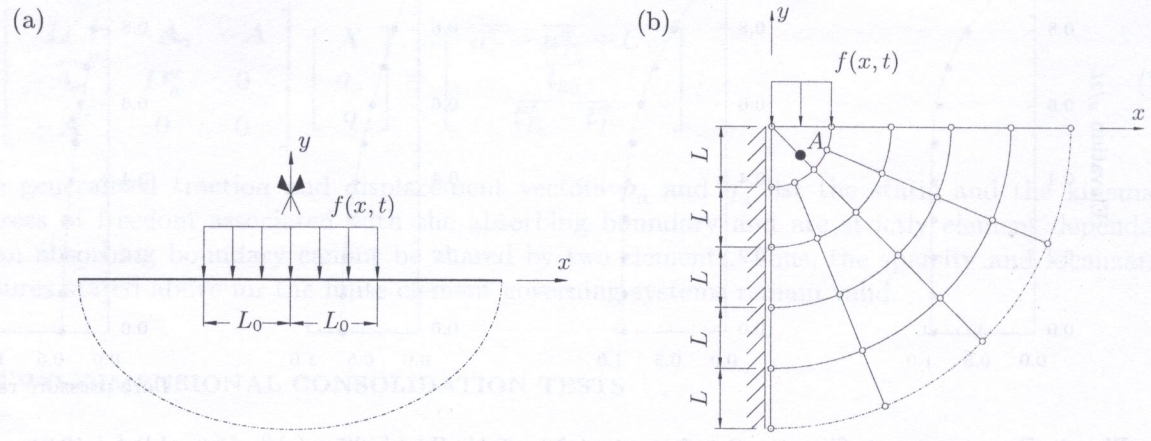

Fig. 5. Physical and finite element model for the unbounded problems; (a) Physical model, (b) Finite element mesh

The simulation implemented in $ABAQUS^{TM}$ is not actually performed on a semi-infinite body of porous saturated soil, as, to the best of the authors' knowledge, the infinite elements there offered are unable to properly model biphasic media (they don't have pore pressure degrees of freedom) [1]. A $50 \times 50\,\mathrm{m}$ medium is, however, considered sufficiently large for the close range stress and pore pressure fields not to be affected by the artificial boundaries and therefore adopted for the analysis. The dimension of a finite element is 25 cm, leading to the discretization of the body into 40 000 finite elements. The 4-node bilinear displacement/pore pressure element CPE4P element is adopted for the analysis. Thus, the total number of structural degrees of freedom is 121 203. The time integration is performed applying a direct method based on the Newton's backward difference formula [1] on 128 time steps.

The time-history of the normalized fluid pore pressure at point $A(1,-1)$, see Fig. 5b, is shown in Fig. 6. Initially, a significant part of the applied traction is supported by the fluid, but the subsequent fluid drainage reduces the magnitude of the pore pressure to about 10% of the applied load at the end of the time interval. A Mandel-Cryer effect is predicted by the hybrid-Trefftz model in the early stages of the analysis, but it is less noticeable in the $ABAQUS^{TM}$ results. Except for the initial instants, however, the two simulations generate similar results.

The normalized pore pressure variation along a vertical plane situated under the applied load ($x = 1$) is presented in Fig. 7 at four selected time points. At the free surface, drainage occurs from the initial phase of the process, causing the pore pressure to be null at all times. Immediately below, however, the drainage is not instantaneous, and the pore pressure increases to about 50% of the applied load (Fig. 7a). The excess pore pressure induces (and is dissipated by) the seepage motion

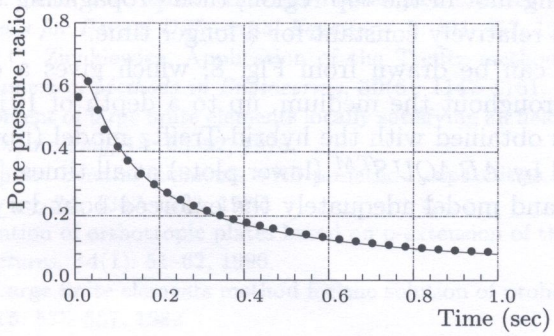

Fig. 6. Pore pressure ratio time history at point A

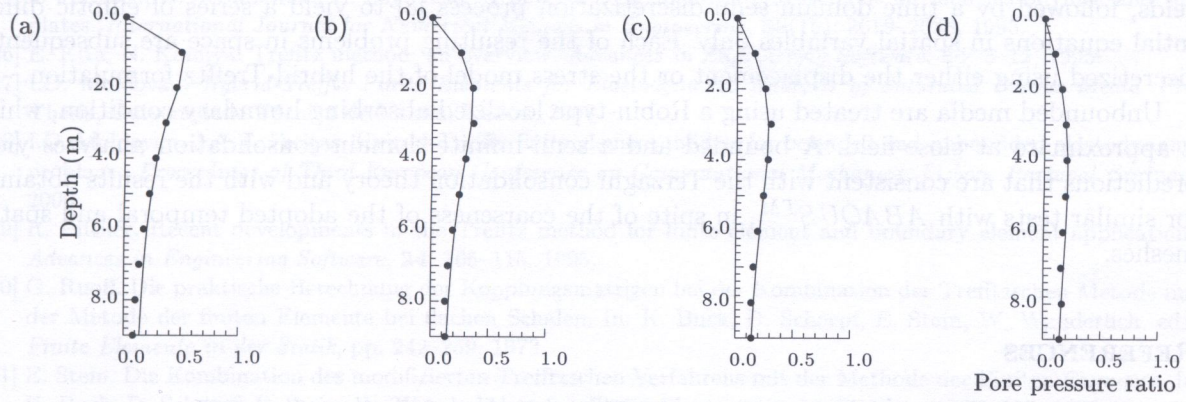

Fig. 7. Pore pressure profiles at selected instants; (a) $t = 0.0625\,\mathrm{s}$, (b) $t = 0.25\,\mathrm{s}$, (c) $t = 0.50\,\mathrm{s}$, (d) $t = 1.0\,\mathrm{s}$

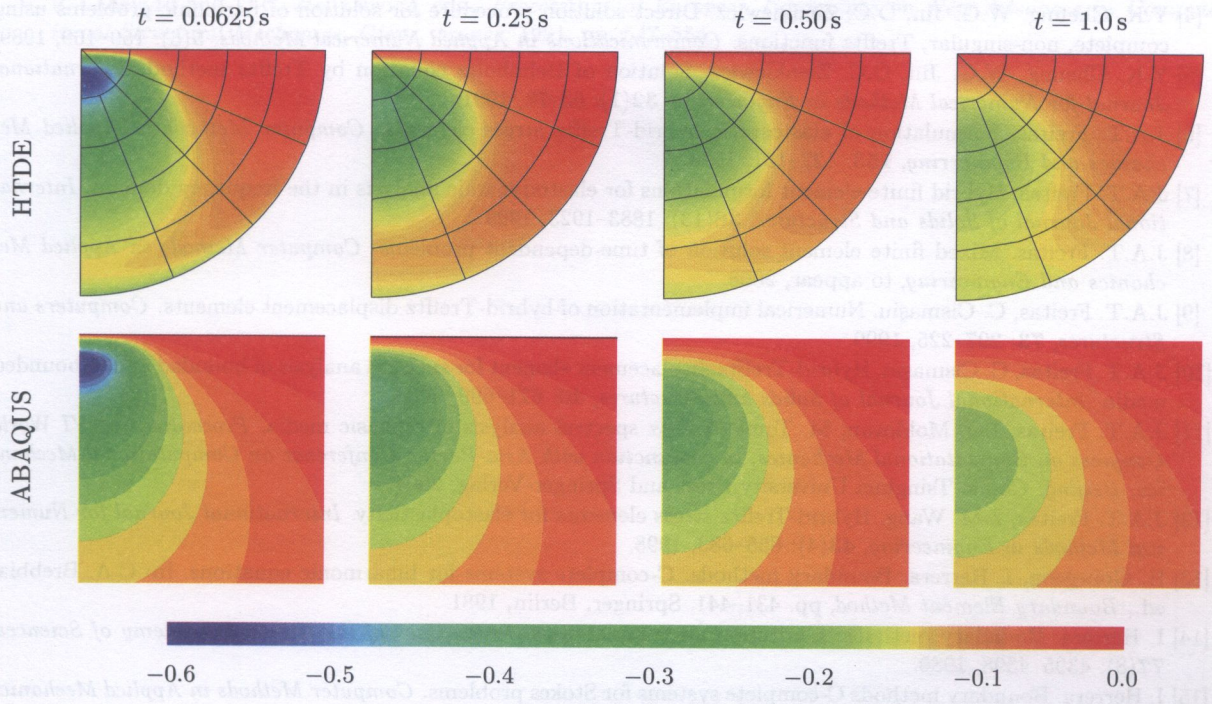

Fig. 8. Pore pressure diagrams at selected time points

of the fluid phase, occurring first in the top region, then propagating towards larger depths, where the pore pressure remains relatively constant for a longer time.

The same conclusions can be drawn from Fig. 8, which gives a color scale representation of the pore pressure field throughout the medium, up to a depth of 10 m at the same instants. The stress/pore pressure fields obtained with the hybrid-Trefftz model (upper plots) are in good agreement with those predicted by $ABAQUS^{TM}$ (lower plots) at all times. They are continuous over the inter-element boundaries and model adequately the enforced boundary conditions.

6. Conclusions

Non-periodic and transient saturated porous media problems are attended here using the displacement and stress models of the hybrid-Trefftz finite element formulation. The integration of the governing equations involves the uncoupling of the temporal and spatial components of the unknown fields, followed by a time domain semi-discretization process [8] to yield a series of elliptic differential equations in spatial variables only. Each of the resulting problems in space are subsequently discretized using either the displacement or the stress model of the hybrid-Trefftz formulation.

Unbounded media are treated using a Robin-type localized absorbing boundary condition, which is approximate at close-field. A bounded and a semi-infinite domain consolidation analyzes yield predictions that are consistent with the Terzaghi consolidation theory and with the results obtained for similar tests with $ABAQUS^{TM}$, in spite of the coarseness of the adopted temporal and spatial meshes.

References

[1] *ABAQUS/Standard. User Manual. Version 5.7.* Hibbitt, Karlsson & Sorensen, Inc., 1997.

[2] M.A. Biot. Theory of propagation of elastic waves in a fluid saturated porous solid. I. Low frequency range. *Journal of Acoustic Society of America*, **28**: 168–178, 1956.

[3] J.P. Carter, J.R. Booker, J.C. Small. The analysis of finite elasto-plastic consolidation. *International Journal of Numerical and Analytical Methods in Geomechanics*, **3**: 107–129, 1979.

[4] Y.K. Cheung, W.G. Jin, O.C. Zienkiewicz. Direct solution procedure for solution of harmonic problems using complete, non-singular, Trefftz functions. *Communications in Applied Numerical Methods*, **5**(3): 159–169, 1989.

[5] Y.K. Cheung, W.G. Jin, O.C. Zienkiewicz. Solution of Helmholtz equation by Trefftz method. *International Journal for Numerical Methods in Engineering*, **32**(1): 63–78, 1991.

[6] J.A.T. Freitas. Formulation of elastostatic hybrid-Trefftz stress elements. *Computer Methods in Applied Mechanics and Engineering*, **153**: 127–151, 1998.

[7] J.A.T. Freitas. Hybrid finite element formulations for elastodynamic analysis in the frequency domain. *International Journal of Solids and Structures*, **36**(13): 1883–1923, 1999.

[8] J.A.T. Freitas. Mixed finite element solution of time-dependent problems. *Computer Methods in Applied Mechanics and Engineering*, to appear, 2008.

[9] J.A.T. Freitas, C. Cismaşiu. Numerical implementation of hybrid-Trefftz displacement elements. *Computers and Structures*, **73**: 207–225, 1999.

[10] J.A.T. Freitas, C. Cismaşiu. Hybrid-Trefftz displacement element for spectral analysis of bounded and unbounded media. *International Journal of Solids and Structures*, **40**: 671–699, 2003.

[11] J.A.T. Freitas, I.D. Moldovan, M. Toma. Trefftz spectral analysis of biphasic media. *Proceedings of VI World Congress on Computational Mechanics, in conjunction with Asia-Pacific Conference on Computational Mechanics, Beijing, China.* Tsinghua University Press and Springer-Verlag, 2004.

[12] J.A.T. Freitas, Z.M. Wang. Hybrid-Trefftz stress elements for elastoplasticity. *International Journal for Numerical Methods in Engineering*, **43**(4): 655–683, 1998.

[13] H. Gourgeon, I. Herrera. Boundary methods. C-complete systems for biharmonic equations. In: C.A. Brebbia, ed., *Boundary Element Method*, pp. 431–441. Springer, Berlin, 1981.

[14] I. Herrera. Boundary methods; a criterion for completeness. *Proceedings of the National Academy of Sciences*, **77**(8): 4395–4398, 1980.

[15] I. Herrera. Boundary methods C-complete systems for Stokes problems. *Computer Methods in Applied Mechanics and Engineering*, **30**: 225–241, 1982.

[16] I. Herrera. *Boundary Methods — an Algebraic Theory.* Pitman Advanced Publishing Program, Boston, 1984.

[17] I. Herrera, R.E. Ewing, M.E. Celia, T.F. Russel. Eulerian-Lagrangian localized adjoint method: the theoretical framework. *Numerical Methods for Partial Differential Equations*, **9**: 431–457, 1993.

[18] W.G. Jin, Y.K. Cheung, O.C. Zienkiewicz. Application of the Trefftz method in plane elasticity problems. *International Journal for Numerical Methods in Engineering*, **30**(6): 1147–1161, 1990.

[19] J. Jirousek. Basis for development of large finite elements locally satisfying all field equations. *Computer Methods in Applied Mechanics and Engineering*, **14**: 65–92, 1978.

[20] J. Jirousek. Hybrid-Trefftz plate bending elements with p-method capabilities. *International Journal for Numerical Methods in Engineering*, **24**: 1367–1393, 1987.

[21] J. Jirousek, M. N'Diaye. Solution of orthotropic plates based on p-extension of the hybrid-Trefftz finite element model. *Computers and Structures*, **34**(1): 51–62, 1990.

[22] J. Jirousek, P. Teodorescu. Large finite elements method for the solution of problems in the theory of elasticity. *Computers and Structures*, **15**: 575–587, 1982.

[23] J. Jirousek, A. Wróblewski. T-elements: state of the art and future trends. *Archives of Computational Methods in Engineering*, **3–4**: 323–434, 1996.

[24] J. Jirousek, A. Wróblewski, X.-Q. He. A family of quadrilateral hybrid-Trefftz p-elements for thick plate analysis. *Computer Methods in Applied Mechanics and Engineering*, **127**(1–4): 315–344, 1995.

[25] J. Jirousek, A. Wróblewski, B. Szybiński. A new 12 DOF quadrilateral element for analysis of thick and thin plates. *International Journal for Numerical Methods in Engineering*, **38**(15): 2619–2638, 1995.

[26] E. Kita, N. Kamiya. Trefftz method: an overview. *Advances in Engineering Software*, **24**: 3–12, 1995.

[27] I.D. Moldovan. *Hybrid-Trefftz Finite Elements for Elastodynamic Analysis of Saturated Porous Media.* PhD Thesis, Universidade Técnica de Lisboa, Lisbon, 2008.

[28] I.D. Moldovan, J.A.T. Freitas. Hybrid-Trefftz finite element models for bounded and unbounded elastodynamic problems. *Proceedings of Third European Conference on Computational Mechanics, Lisbon, Portugal.* Springer, 2006.

[29] R. Piltner. Recent developments in the Trefftz method for finite element and boundary element applications. *Advances in Engineering Software*, **24**: 105–115, 1995.

[30] G. Ruoff. Die praktische Berechnung der Kopplungsmatrizen bei der Kombination der Trefftzschen Metode und der Metode der finiten Elemente bei flachen Schalen. In: K. Buck, D. Scharpf, E. Stein, W. Wunderlich, eds., *Finite Elemente in der Statik*, pp. 242–259, 1973.

[31] E. Stein. Die Kombination des modifizierten Trefftzschen Verfahrens mit der Methode der Finiten Elemente. In: K. Buck, D. Scharpf, E. Stein, W. Wunderlich, eds., *Finite Elemente in der Statik*, pp. 172–185, 1973.

[32] K. Terzaghi, R.B. Peck. *Soil Mechanics in Engineering Practice.* John Wiley and Sons, New York, 1948.

[33] E. Trefftz. Ein Gegenstuck zum Ritzschen Verfahren. *Proceedings of The International Congress of Applied Mechanics*, Zurich, 1926, pp. 285–292.

[34] G.M. Vörös, J. Jirousek. Application of the hybrid-Trefftz finite element model to thin shell analysis. In: P. Ladeveze and O.C. Zienkiewicz, eds., *Proceedings of European Conference on New Advances in Computational Structural Mechanics, Giens, France*, 1991, pp. 547–554.